Hole transport properties in gallium antimonide from 77 to 300°K

P. C. Mathur and Sushil Jain
Department of Physics and Astrophysics, University of Delhi, Delhi-110007, India
(Received 19 December 1977)

Hall-mobility and transverse-magnetoresistance measurements have been made on zinc-doped p-GaSb from 77 to 300°K. Single-crystal samples with doping concentrations 8×10^{17} and 3×10^{18} cm^{-3} were investigated. The split in the heavy- and light-hole bands due to the influence of the linear k term in the energy expression of the holes in the valence band has been investigated. An energy separation of 0.015 eV has been found to explain the observed galvanomagnetic data. Intervalley and intravalley scattering by the acoustical, nonpolar, and polar-optical phonons and the ionized-impurity scattering for p-like wave functions in the valence band have been considered. The impurity activation energy associated with the heavy-hole band is found to be 0.010 eV in the lightly doped sample. The impurity band is shown to merge with the valence band in the more heavily doped p-GaSb.

I. INTRODUCTION

The energy-wave-vector relation for holes in III-V compounds, including GaSb, contains a linear-k term introduced owing to lack of inversion symmetry in their crystal structure, by the spin-orbit splitting. As shown by Dresselhaus,[1] because of the linear-k term, the light- and heavy-hole bands are split into two nondegenerate bands, and the energy maxima of the valence bands are not at $k(0,0,0)$. Experimental evidence for their existence has been obtained from free-carrier absorption in GaAs by Braunstein[2] and in InAs by Matossi and Stern.[3] The influence of the linear-k term on the shape of the isoenergetic surfaces in p-GaSb has been deduced by Robert *et al.*[4] from galvanomagnetic measurements. They have shown that the nonquadratic-band model of Lax and Mavroides[5] for germanium and silicon is insufficient to account for all the observed galvanomagnetic phenomena. They have, in fact, determined the anisotropy coefficients of the light- and heavy-hole ellipsoids along the [100] and [111] directions to be 1.66 and 3, respectively.

In the present work, we have determined the energy difference between the valence-band maxima for heavy and light holes, by fitting the theoretically calculated Hall coefficient, conductivity, and transverse magnetoresistance with the experimental results. The experiment has been performed on single-crystal samples of p-GaSb doped with zinc and having carrier concentrations of 6×10^{17} and 3×10^{18} cm^{-3} at 300°K, respectively. In the mobility analysis inter- and intravalley scattering by acoustical, polar, and nonpolar phonons, and ionized impurities, of holes having p-like symmetry has been included. In the lightly doped sample at low temperatures the dominant contribution is from ionized-impurity scattering. In the more heavily doped sample, however, impurity-band conduction is assumed to be present in addition to ionized-impurity scattering, in order to interpret the low-temperature mobility data. Near room temperature all four scattering mechanisms are shown to be important. The activation energy of the zinc acceptors has been found to be 10 meV in the lightly doped sample, while the impurity band merges with the valence band in the heavily doped case. The impurity level associated with the light-hole band has been assumed to be merged with it owing to the very low effective mass.

II. EXPERIMENT

Zinc-doped single-crystal slices of gallium antimonide, grown from stoichiometric melt have been used for the measurement of the Hall coefficient R_H, the conductivity σ, and the transverse magnetoresistance $\Delta\rho/\rho$ on p-GaSb. The samples were cut perpendicular to the [111] direction from two single-crystal boules labeled I and II and having acceptor densities of 8×10^{17} and 3×10^{18} cm^{-3}, respectively, at room temperature as determined from the Hall-coefficient data. Both samples I and II are disk shaped with average diameters of 1.6 and 1.0 cm, respectively, and thickness 0.1 cm each. The Van der Pauw technique[6] has been used for the measurement of the magnetoresistivity and Hall coefficient. Four-point contacts of average size 0.5 mm were alloyed (with Sn, Zn alloy) on the periphery of the samples. The error due to the finite size of the contacts is less than 3%. A Keithley nanovoltmeter has been used to measure Hall voltages and the fractional change in resistivity on application of the magnetic field with an accuracy of one in a thousand. The directions of the magnetic field and the current were reversed in order to eliminate errors due to thermoelectric and thermomagnetic effects. The

temperature variation was recorded by keeping the sample in a Dewar over the liquid-nitrogen surface. As the nitrogen evaporated, the temperature increased slowly enough to allow a set of four readings within 1 °K. The temperature over the surface of the sample was also checked to be uniform to within 1 °K. The maximum applied magnetic field is 0.3 T, measured with an accuracy of 2%, as $\Delta\rho/\rho B^2$ remained constant below this field. The influence of the anisotropic nature of the valence bands has been neglected since the angular variation of the magnetoresistance as reported by Becker *et al.*[7] is only about 5%, which is the limit of the accuracy with which the magnetoresistance has been measured in the present work.

III. VALENCE-BAND STRUCTURE AND THE CARRIER DISTRIBUTION

Dresselhaus[1] showed in the case of III-V compounds that the energy has the form

$$E = E_v \pm c\left\{k^2 \pm \left[3(k_x^2k_y^2 + k_y^2k_z^2 + k_z^2k_x^2)\right]^{1/2}\right\}^{1/2}. \quad (1)$$

The linear-k term in the above expression lifts the degeneracy of light- and heavy-hole bands at $k=0$. As shown by Robert *et al.* the energy maxima are located on the ⟨111⟩ and ⟨100⟩ axes with the isoenergetic surfaces as ellipsoids of revolution. They estimate empirically the energy of the heavy-hole band extremum to be 0.020 eV above that at $k=0$. According to Matossi and Stern, for light holes this energy may be one-third as large as for the heavy-holes band and the effect of the linear-k term cannot be neglected.

Zinc acceptors produce N_A levels associated with the heavy-hole band, N_A being the concentration of acceptor impurities, and have an ionization energy E_A. The carrier concentrations p_1 and p_2 in the light- and heavy-hole bands, respectively, are related to N_A and E_A by the relation

$$p_1 + p_2 + \frac{N_A}{1 + (1/g_A)e(E_A - E_F)/k_BT} = N_A. \quad (2)$$

Here, E_F is Fermi energy referred to the energy maximum of the heavy holes and g_A is the degeneracy factor of the impurity levels. p_1 and p_2 can be found from the density of states and the Fermi energy as

$$p_1 = \frac{1}{\pi^2}\left(\frac{2m_{d1}^* k_BT}{\hbar^2}\right)^{3/2} F_{1/2}\left(\frac{E_F - \Delta E}{k_BT}\right), \quad (3)$$

$$p_2 = \frac{1}{\pi^2}\left(\frac{2m_{d2}^* k_BT}{\hbar^2}\right)^{3/2} F_{1/2}\left(\frac{E_F}{k_BT}\right), \quad (4)$$

where m_{d1}^* and m_{d2}^* are the equivalent density-of-state effective masses of light and heavy holes, respectively. ΔE is the energy separation between the energy maxima of the two types of holes.

IV. SCATTERING MECHANISMS OF THE CHARGE CARRIERS

Due to the p-like symmetry of the valence bands, the relative contribution of the different scattering mechanisms is quite different as compared to that for electrons in the polar III-V compound semiconductors. A number of papers have appeared recently to clarify the relative importance of acoustical, nonpolar, and polar optical-phonon scatterings in p-type polar semiconductors.[8-11] A review of these results and a comparison with experiment were given by Kranzer.[12]

The overlap correction, introduced in the acoustical-phonon scattering rate by the p-like symmetry of the valence-band wave functions, is to enhance the relaxation time by a factor of 2 over the case in which the overlap is omitted as has been shown by Wiley.[13] Since the deformation-potential constant itself has been determined by treating it as an adjustable parameter, the expression for the relaxation time for acoustical-phonon scattering valid for s-like symmetric wave functions has been used,[12]

$$\tau_{ac}^{-1} = \frac{\sqrt{2}E_{ac}^2 m_d^{*3/2} k_BT}{\pi\hbar^4\rho\bar{u}^2} E^{1/2}, \quad (5)$$

where $\bar{u}$ is the average sound velocity in the semiconductor of mass density ρ and F_{ac} is the deformation-potential constant. The momentum relaxation time for nonpolar-optical-phonon scattering valid for p-like wave functions is given by[12]

$$\tau_{npo}^{-1} = \frac{E_{npo}^2\hbar\omega_0 m_d^{*3/2}}{\sqrt{2}\pi\hbar^4\rho\bar{u}^2} \times \left[N_0(E+\hbar\omega_0)^{1/2} + \mathrm{Re}(E-\hbar\omega_0)^{1/2}(N_0+1)\right], \quad (6)$$

where $\hbar\omega_0$ is the optical-phonon energy and E_{npo} is the optical-deformation-potential constant. In the case of polar-optical-phonon scattering, the problem of the failure of the relaxation-time approach has been overcome by using numerical methods[14] for treating several n-type compound semiconductors. Kranzer[12] has solved numerically a set of coupled inhomogeneous difference equations and has modified the mobility expression of Howarth and Sondheimer[15] originally calculated for carriers having s-like symmetry. Based on this mobility expression, the following relaxation time for polar-optical-phonon scattering has been used:

$$\tau_{po} = \frac{(m_d^* k_BT/2)^{1/2}}{eE_{po}N_0}\chi\left(\frac{\Theta_D}{T}\right)E^{1/2}, \quad (7)$$

where

$$E_{po} = m_d^* e\omega_0/\hbar(\epsilon_\infty^{-1} - \epsilon_0^{-1}).$$

N_0 is the number of optical phonons and is equal

to $[\exp(\Theta_D/T)-1]^{-1}$ Θ_D is the Debye temperature, equal to $\hbar\omega_0/k_B$, ϵ_∞ and ϵ_s are the high-frequency and static dielectric constants. $\chi(\Theta_D/T)$ is modified for p-like wave function carriers. The modified values are tabulated in Table I.

The scattering by ionized impurities has been described[12] by the modified Brooks-Herring theory accounting for the p-like wave function of the holes. For spherical bands, the momentum relaxation time is given by[12]

$$\tau_{\text{ion}}^{-1}=\pi e^4 N_i \Phi(z) E^{-3/2}/\epsilon_s^2 (2m_d^*)^{1/2}, \tag{8}$$

where

$$\Phi(z)=\frac{1}{4}\left[(1-3z)^2\ln\left|\frac{1+z}{1-z}\right|+\frac{z}{1+z}(2-3z-qz^2)\right],$$

$$z=1+\hbar^2 p_2 e^2/4m_d^* E\epsilon k_B T. \tag{9}$$

N_i is the total number of ionized scatterers and is equal to p_1+p_2. While considering scattering of light holes, N_i becomes p_1+2p_2 in order to include scattering by heavy holes.

Owing to the close proximity of light- and heavy-hole bands, intervalley and intravalley scatterings occur. The intervalley scattering affects the mobility of light holes appreciably. Hence it drastically influences the low-field galvanomagnetic properties. It is not difficult to see that interband scattering requires a large change in the wave vector $\vec{k}$. Hence these transitions can be caused by the acoustical and the optical phonons and not by the ionized impurities. Furthermore, because of the large density of states in the heavy-hole band, a comparatively small number of light holes will be frequently scattered into the heavy-hole band. Hence scattering by the intervalley acoustical or the optical phonons predominates in the light-hole band whereas it is negligible in the heavy-hole band.

The total relaxation time for heavy holes, τ_2, is thus obtained by adding the respective relaxation times of the four processes as discussed above, taking m_d^* equal to the heavy-hole density-of-states effective mass (m_{d2}^*) signifying intraband scattering only. For the total relaxation times of the light holes, τ_1, the individual relaxation times have been similarly added, taking $m_d^*=m_{d2}^*$ for lattice scattering processes and m_{d1}^* for the ionized-impurity scattering signifying interband and intraband scattering, respectively. The relaxation times τ_1 and τ_2 are averaged over the Fermi-Dirac distribution of energy of the carriers as

$$\langle\tau\rangle=\int_0^\infty \tau\left(-\frac{\partial f_0}{\partial E}\right)E^{3/2}\,dE \Big/ \int_0^\infty \left(-\frac{\partial f_0}{\partial E}\right)E^{3/2}\,dE, \tag{10}$$

where f_0 is the Fermi factor, equal to $\{1+\exp[(E-E_F)/k_BT]\}^{-1}$.

TABLE I. Values of $\chi(\Theta_D/T)$.

Θ_D/T	0	1	3	5	8
$\chi(\Theta_D/T)$	1.8	1.4	2.4	3.3	4.2

V. THEORETICAL EXPRESSIONS FOR HALL COEFFICIENT AND MAGNETORESISTANCE

The Hall coefficient R_H and conductivity σ in a two-band conduction process depend more strongly on the magnetic field compared with the single-band conduction process. In the limit of low magnetic fields, however, R_H and $\Delta\rho/\rho B^2$ are independent of the field. The expressions for R_H and $\Delta\rho/\rho B^2$ involving the carrier concentrations p_1, p_2, and the relaxation times τ_1 and τ_2 are given by[16]

$$R_H=\sum_i \frac{p_i e^3\langle\tau_i^2\rangle F(K_i)}{m_{ic}^{*2}} \Big/ \left(\sum_i \frac{p_i e^2\langle\tau_i\rangle}{m_{ic}^*}\right)^2, \tag{11}$$

$$\frac{\Delta\rho}{\rho B^2}=\frac{\sum_i \frac{p_i e^4\langle\tau_i^3\rangle F(K_i)}{m_{ic}^{*3}}\sum_i \frac{p_i e^2\langle\tau_i\rangle}{m_{ic}^*}-\left(\sum_i \frac{p_i e^3\langle\tau_i^2\rangle F(K_i)}{m_{ic}^{*2}}\right)^2}{\left(\sum_i \frac{p_i e^2\langle\tau_i\rangle}{m_{ic}^*}\right)^2}, \tag{12}$$

where

$$F(K_i)=3K_i(K_i+2)/(2K_i+1)^2.$$

m_{ic}^* and K_i are the conductivity effective mass and its band anisotropy in the ith band.

In terms of the mobilities μ_1 and μ_2, Eq. (11) can be written

$$R_H=\frac{p_1\mu_1^2 r_1+p_2\mu_2^2 r_2}{e(p_1\mu_1+p_2\mu_2)^2}, \tag{13}$$

where

$$r_i=\langle\tau_i^2\rangle F(K_i)/\langle\tau_i\rangle^2 \quad (i=1,2).$$

Equation (12) also acquires a very simple form in terms of μ_1, μ_2, r_1, and r_2 under the assumption that $\langle\tau^3\rangle\langle\tau\rangle/\langle\tau^2\rangle^2$ equals unity, which is usually true to within a few percent, and can be written

$$\frac{\Delta\rho}{\rho B^2}=\frac{\mu_1\mu_2(p_1/p_2)[1-(r_1/r_2)(\mu_1/\mu_2)]^2}{[1+(p_1/p_2)(\mu_1/\mu_2)]^2}. \qquad (14)$$

VI. HALL-COEFFICIENT AND MAGNETORESISTANCE CALCULATION METHOD

All the computations, including the evaluation of integrals as in Eq. (10) and the solution of transcendental equations such as (2), have been done numerically on an IBM 360-44 computer. The values of the material parameters used in the theoretical calculations are given in Table II. The values of anisotropy factors K_1 and K_2, used in the calculations, have also been taken from the same table. To start with, approximate values of N_A, E_A, and ΔE are assumed and Eq. (2) is solved for E_F by the Mullers iterative technique.[17] Once E_F is known p_1 and p_2 are also known from Eqs. (3) and (4). The concentration of the ionized acceptors N_I is then equal to p_1+p_2. The average relaxation times $\langle\tau_1\rangle$ and $\langle\tau_2\rangle$ and their higher powers such as $\langle\tau_1^2\rangle$, etc. for light and heavy holes are evaluated from Eq. (10). Hence Eqs. (11) and (12) give easily the values of R_H and σ. For a set of values of N_A, E_A, and ΔE, R_H, σ, and $\Delta\rho/\rho B^2$ are calculated as functions of temperature and compared with their experimental values. In this way a set of values for N_A, E_A, and ΔE has been obtained which gives the best agreement between theoretical and experimental results.

VII. RESULTS AND DISCUSSIONS

The variation of the conductivity and Hall coefficient with temperature, obtained experimentally, is shown in Fig. 1 by data points for samples I and II, respectively. The continuous curves in the figure are the theoretical best fit. R_H slowly decreases with increasing temperature for sample I which has less doping signifying ionization of holes into the valence band from an associated impurity level. In the more heavily doped sample II R_H remains constant with temperature. This is typical of impurity band merging with valence band. Welker[18] also obtained similar results for R_H in heavily doped samples.

Corresponding to the best fit of the experimental results for R_H and σ, the theoretical calculations yield the activation energy of the zinc acceptors (E_A) as 10 meV and 0 eV for samples I and II with N_A equal to 8×10^{17} and 3×10^{18} cm^{-3}, respectively. Assuming the hydrogenic nature of zinc impurities one gets an activation energy of 21 meV according to the expression $13.6\times m_d^*/\epsilon_s^2$. At low-doping density, E_A for zinc impurities has been found to be 37 meV.[13]

The lower values of E_A, as obtained in the present work, can be explained as an effect of increased doping. At higher impurity concentrations (~10^{18} cm^{-3}) the impurity energy levels tend to merge with the conduction band.[20] Therefore, at acceptor concentration of 8×10^{17} cm^{-3} an activation energy of 10 meV is obtained and at 3×10^{18} cm^{-3} doping density the impurity level merges with the heavy-hole band, i.e., the impurity ac-

TABLE II. Physical constants of the material.

Light-hole effective mass, m_{1d}^*	$0.05\,m_0$[1] [a]
Heavy-hole effective mass, m_{2d}^*	$0.35\,m_0$ [a]
Density, ρ	5.6137 [b] g/cm^3
Average sound velocity, $\bar{u}$	3.24×10^5 [c] cm/sec
Acoustical deformation-potential constant, E_{ac}	4.0 eV [a]
Nonpolar optical deformation-potential constant, E_{npo}	6.0 eV [a]
Optical-phonon energy, $\hbar\omega_0$	0.0297 eV [d]
Optical dielectric constant, ϵ_∞	13.8 [d]
Static dielectric constant, ϵ_s	15.0 [d]
Degeneracy factor of impurity levels, g_A	2 [e]
Light-hole anisotropy factor, K_1	1.66 [f]
Heavy-hole anisotropy factor, K_2	3.00 [f]

[a] From Ref. 12.
[b] From Ref. 13.
[c] From Ref. 11.
[d] From Ref. 24.
[e] From Ref. 19.
[f] From Ref. 4.

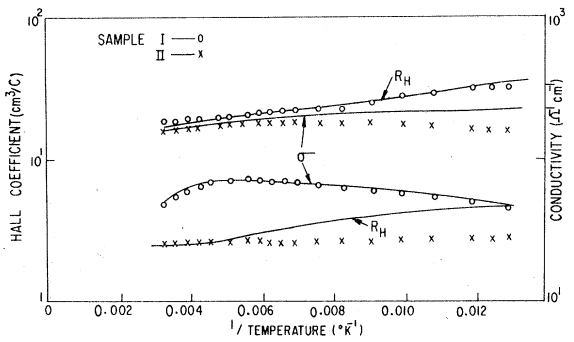

FIG. 1. Experimental points of Hall coefficient and conductivity for sample I (O) and sample II (×) are shown as a function of temperature. The continuous curves are the theoretical best fit.

tivation energy reduces to zero. A decrease of E_A with increasing doping in p-GaSb has been observed by Van Mau *et al.*[21] The formation of impurity bands leads to tailing of the density of states into the forbidden gap near the zone center and the dispersion relation for the carrier energy is modified.[22] The poor fit of theory and experiment for sample II at low temperatures is clearly due to these impurity-band effects. At higher temperatures, however, due to the larger carrier energies, these effects are minimized.

The variation of the Fermi energy and of the heavy- to light-hole concentration ratio, i.e., p_2/p_1, with temperature is shown in Fig. 2. These curves correspond to $\Delta E = 0.015$ eV. The ratio p_2/p_1 becomes very high at low temperatures in sample I because of the very low density of states in the light-hole band and energy separation ΔE which the carriers are required to have to be excited from the upper heavy-hole band to the lower light-hole band. In sample II, however, p_2/p_1 does not become that high because of the degeneracy of the valence bands. The Fermi level lies within the light-hole band at 77 °K and is easily populated. Near room temperature also, due to the higher thermal energy of the carriers which is even greater than ΔE, the light-hole band gets easily populated and p_2/p_1 does not become very high.

Figure 3 shows the mobilities, combined for light and heavy holes according to Eq. (13), separately for the three lattice scattering mechanisms discussed, i.e., acoustical, polar, and nonpolar optical phonons. Nonpolar scattering can be seen to be dominant over the others including ionized-impurity scattering (see Fig. 4) at 300 °K in sample I. Acoustical and polar contributions to the scattering decrease owing to the p-like nature of the carrier wave functions. At 77 °K only ionized-impurity scattering exists. In Fig. 4, the light- and heavy-hole intraband-ionized-impurity-scattering limited mobilities are shown. In sample II, the ionized-impurity scattering remains most significant at all temperatures. The saddle-shaped curve in this figure indicates that the screening term becomes more dominant at lower

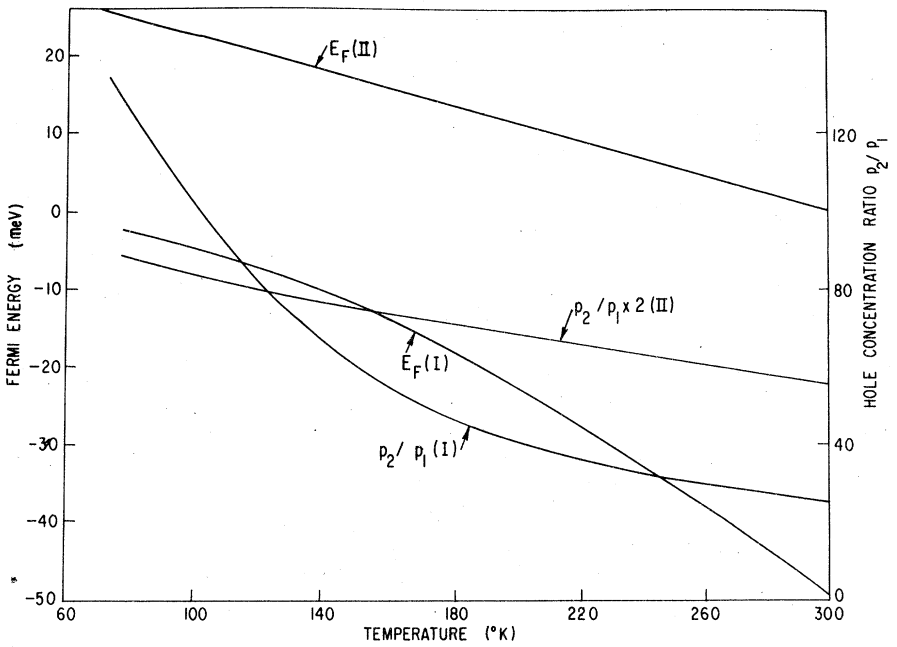

FIG. 2. Concentration ratio p_2/p_1 of heavy and light holes and the Fermi energy in samples I and II are shown as a function of temperature.

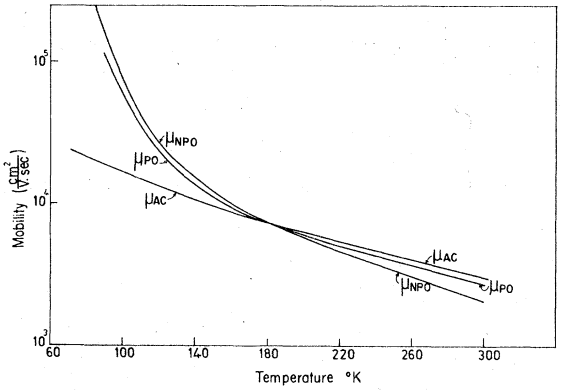

FIG. 3. Temperature variation of the mobilities due to acoustical, nonpolar, and polaroptical phonons. These mobilities are combined for light and heavy holes according to Eq. (13).

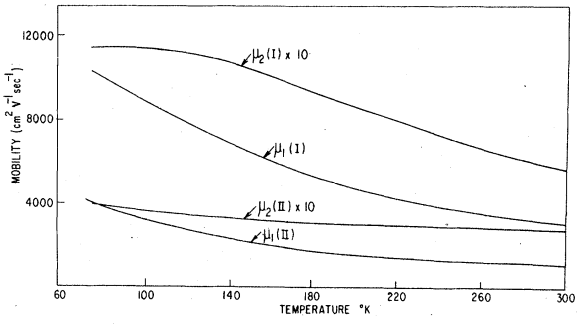

FIG. 5. Total light- and heavy-hole mobilities μ_1 and μ_2 as a function of temperature.

temperatures than the $T^{3/2}$ term in the relaxation time of ionized impurities. The $T^{3/2}$ behavior of the ionized-impurity mobility appears at higher temperatures. The screening term becomes even more significant for the light holes and therefore the light- to heavy-hole mobility ratio increases with decrease in temperature. Figure 5 shows the temperature variation of the total light- and heavy-hole mobilities. The total effective mobility and the experimental mobilities for the two samples are shown in Fig. 6. The agreement is not good for sample II at lower temperatures. This is because of the fact that the impurity-band conduction in this heavily doped sample becomes quite significant as mentioned earlier.

Finally $\Delta\rho/\rho B^2$ as calculated theoretically from Eq. (12) is compared with the experimental results in Fig. 7. The experimental value of $\Delta\rho/\rho B^2$ at 77 K for sample I is comparable to that obtained by Becker *et al.*[7] Had the valence bands been assumed degenerate at $k=0$, the theoretical values of $\Delta\rho/\rho B^2$ for sample I would have been much lower than the presently calculated results. In fact, the decrease in $\Delta\rho/\rho B^2$ with temperature increase is due to the decrease in the value of the mobility ratio of light and heavy holes and of the heavy- to light-hole population ratio. In sample II, though the mobility is low, the high magnetoresistance at 77 K is understandable due to the large value of

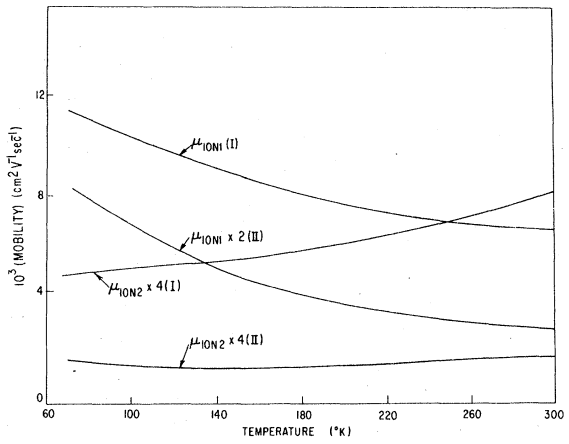

FIG. 4. Intravalley scattering due to ionized impurities for the light and heavy holes.

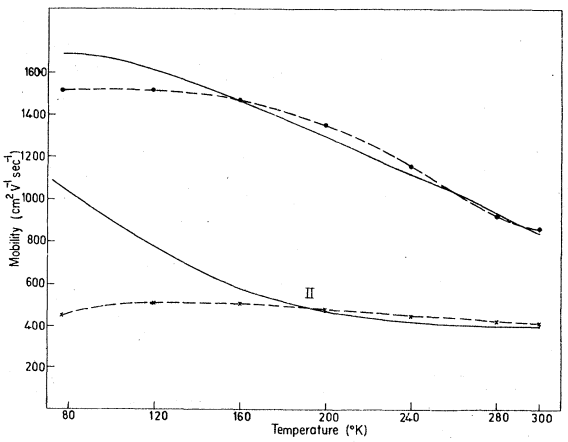

FIG. 6. Total effective mobility μ as calculated theoretically (dashed curve) and also experimentally ($R_H\sigma$) (continuous curve) for samples I and II.

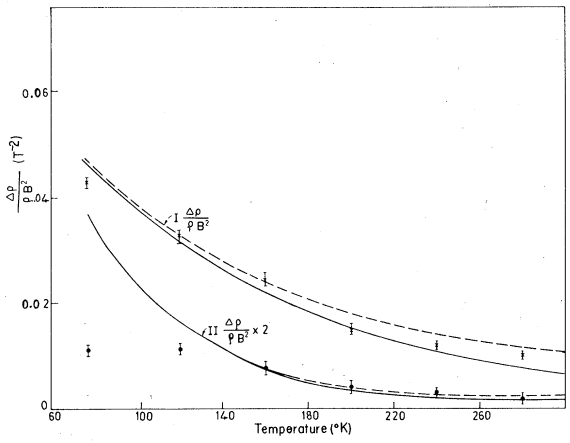

FIG. 7. Transverse magnetoresistance $\Delta\rho/\rho B^2$ at a magnetic field of 0.3 T is plotted vs temperature for samples I and II. The continuous curve is the one calculated according to Eq. (12), and the dashed curve is calculated from Eq. (14). ● are experimental points within error bars.

μ_1/μ_2, the light- to heavy-hole mobility ratio. Near room temperature, since μ_1/μ_2 decreases, $\Delta\rho/\rho B^2$ becomes very small. Also shown in Fig. 7 for comparison are the curves calculated using Eq. (14).

VIII. CONCLUSIONS

The splitting of the energy maxima of the heavy and light holes has been found to be 0.015 eV. Due to this split, the concentration ratio p_2/p_1 of heavy and light holes varies with temperature. Ionized-impurity scattering, including the scattering of the light holes by the heavy holes, has been shown to be the dominant scattering mechanism at low temperatures in the two samples studied. The mobility ratio μ_1/μ_2 of the light to heavy holes is found to vary with temperature. The inclusion of the variation of p_2/p_1 and μ_1/μ_2 with temperature yields calculated curves fitting the measured transverse magnetoresistance, except at low temperatures in the more heavily doped sample, where impurity-band effects (not included in the theoretical analysis) are expected to be important.

[1]G. Dresselhaus, Phys. Rev. 100, 580 (1955).
[2]R. Braunstein and E. O. Kane, J. Phys. Chem. Solids 23, 1023 (1962).
[3]F. Matossi and F. Stern, Phys. Rev. 111, 472 (1958).
[4]J. L. Robert, B. Pistoulet, D. Barjon, and A. Raymond, J. Phys. Chem. Solids 34, 2221 (1973).
[5]J. G. Mavroides and B. Lax, Phys. Rev. 107, 1530 (1957).
[6]L. J. Van der Pauw, Phillips. Tech. Rev. 20, 230 (1958).
[7]W. M. Becker, A. K. Ramdas, and H. Y. Fan, J. Appl. Phys. 32, 2094 (1961).
[8]M. Costato, G. Jacobini, and L. Reggiani, Phys. Status. Solidi B 52, 461 (1972).
[9]D. Kranzer, J. Phys. C 6, 2977 (1973).
[10]D. Kranzer, J. Phys. C 6, 2967 (1973).
[11]I. D. Wiley and D. DiDomenico, Phys. Rev. B 2, 427 (1970).
[12]D. Kranzer, Phys. Status Solidi A 26, 11 (1974).
[13]I. D. Wiley, Phys. Rev. B 4, 2485 (1971).
[14]D. L. Rode, Phys. Rev. B 2, 1012 (1970).
[15]D. J. Howarth and E. H. Sondheimer, Proc. R. Soc. A 219, 53 (1953).
[16]K. Seeger, *Semiconductor Physics* (Springer-Verlag, New York, 1972), pp. 75–76.
[17]G. K. Kristiansen, Nordisk Tidskr. Informations Behandling (BIT) 3, 205–206 (1963).
[18]H. Welker, J. Electron. 1, 181 (1954).
[19]H. Welker, Physica 26, 843 (1954).
[20]G. L. Pearson and J. Bardeen, Phys. Rev. 75, 865 (1949).
[21]A. N. Van Mau, M. Averous, and G. Bougnot, C. R. Acad. Sci. B 271, 900 (1970).
[22]V. I. Bonch-Bruyevich, *The Electric Theory of Heavily Doped Semiconductors* (American Elsevier, New York, 1966).
[23]J. Basinski, S. D. Rosenbaum, S. L. Basinski, and J. C. Woolley, J. Phys. C 6, 422 (1973).
[24]J. Basinski, D. J. E. Demars, and J. C. Woolley, J. Phys. C 7, 716 (1974).